IAEA
International Atomic Energy Agency

20th IAEA Fusion Energy Conference
Vilamoura, Portugal, 1 to 6 November 2004

IAEA-CN-116/EX/P2-21

OPTIMIZING THE BETA LIMIT IN DIII-D ADVANCED TOKAMAK DISCHARGES

J.R. FERRON, T.A. CASPER,[1] E.J. DOYLE,[2] A.M. GAROFALO,[3] P. GOHIL, C.M. GREENFIELD, A.W. HYATT, R.J. JAYAKUMAR,[1] C. KESSEL,[4] T.C. LUCE, M.A. MAKOWSKI,[1] J.E. MENARD,[4] M. MURAKAMI,[5] C.C. PETTY, P.A. POLITZER, T.S. TAYLOR, and M.R. WADE[5]

General Atomics
San Diego, California 92186-5608
United States of America

[1]Lawrence Livermore National Laboratory, Livermore, California, USA
[2]University of California, Los Angles, Los Angeles, California USA
[3]Columbia University, New York, New York
[4]Princeton Plasma Physics Laboratory, Princeton, New Jersey, USA
[5]Oak Ridge National Laboratory, Oak Ridge, Tennessee, USA

Optimizing the Beta Limit in DIII-D Advanced Tokamak Discharges

J.R. Ferron,[1] T.A. Casper,[2] E.J. Doyle,[3] A.M. Garofalo,[4] P. Gohil,[1] C.M. Greenfield,[1] A.W. Hyatt,[1] R.J. Jayakumar,[2] C. Kessel,[5] T.C. Luce,[1] M.A. Makowski,[2] J. Menard,[5] M. Murakami,[6] C.C. Petty,[1] P.A. Politzer,[1] T.S. Taylor,[1] and M.R. Wade[6]

[1]General Atomics, P.O. Box 85608, San Diego, California 92186-5608, USA
email: ferron@fusion.gat.com
[2]Lawrence Livermore National Laboratory, Livermore, California, USA
[3]University of California, Los Angles, Los Angeles, California USA
[4]Columbia University, New York, New York
[5]Princeton Plasma Physics Laboratory, Princeton, New Jersey, USA
[6]Oak Ridge National Laboratory, Oak Ridge, Tennessee, USA

Abstract. Results are presented from comparisons of modeling and experiment in studies to assess the best choice of safety factor (q) profile, pressure profile and discharge shape for high beta, steady-state, noninductive advanced tokamak operation. This is motivated by the need for high $q_{\min}\beta_N$ to maximize the self-driven bootstrap current while maintaining high toroidal beta to increase fusion gain. Experiment and theory both show that increases in the achievable normalized beta (β_N) can be obtained through broadening of the pressure profile and use of a symmetric double-null divertor shape. The general trend is for β_N to decrease as the minimum q value ($q_{\min}$) increases, but with a broadened pressure profile, $\beta_N = 4$ is obtained with $q_{\min} \approx 2$ and $q_{\min}\beta_N$ increases with $q_{\min}$. Modeling of equilibria with near 100% bootstrap current indicates that operation with $\beta_N \approx 5$ should be possible with a sufficiently broad pressure profile.

1. Introduction

This paper describes the investigation of methods to facilitate steady-state operation in DIII-D advanced tokamak discharges [1] by maximizing $q_{\min}\beta_N$. The interest in this quantity arises because steady-state tokamak operation requires 100% of the plasma current to be driven noninductively, which is best achieved with a high fraction of self-driven bootstrap current, $f_{BS} \propto \beta_P \propto q\beta_N$.This motivates operation with elevated safety factor (q) values across the entire profile. However, in order to maintain high fusion gain, $\propto \beta\tau_E \propto \beta_N H_{89}/q_{95}^2$, $q\beta_N$ should be optimized by increasing the minimum q value ($q_{\min}$) rather than q near the plasma boundary, q_{95}. To achieve high fusion gain and maximize f_{BS}, operation at the highest possible value of the normalized toroidal beta (β_N) is required. Here $\beta_N = \beta aB/I$ where I is the total plasma current, a is the minor radius and B is the toroidal field strength.

The efforts to maximize $q_{\min}\beta_N$ in DIII-D have focused on modifications of the present steady-state advanced tokamak scenario. In this scenario [2,3], $1.5 < q_{\min} < 3$, $q_{95} \approx 5$, $\beta_N = 3.2$ to 3.5 and $q_{\min}\,\beta_N \approx 6$. As described in Section 2, the maximum achievable β_N is observed to decrease as $q_{\min}$ is increased without modification of the pressure profile. Consistent with this observation, the β_N limit for stability to ideal, low toroidal number (n) modes without a conducting wall is measured and calculated to decrease as $q_{\min}$ is increased. In Section 3, it is shown that modeling of equilibria with near 100% bootstrap current indicates that $\beta_N = 5$ should be stable with a sufficiently broad pressure profile. In the experiment, when the pressure profile is broadened by increasing the density profile width, the maximum β_N increases from 3.5 to 4 with the minimum q value above 2 and the resulting maximum $q_{\min}\beta_N \approx 9$. The discharge shape for DIII-D steady-state research is presently chosen to make best use of the cryopumping available in the upper divertor region in order to minimize the electron density for efficient off-axis electron cyclotron current drive and allow operation at collisionalities relevant to burning plasma and beyond. Thus a single-null divertor shape is used in order to direct exhaust particles to the upper divertor. The triangularity is chosen to best match the cryopump geometry. As discussed in Section 4, both experiment and modeling show that it is possible to increase β_N through modifications to this discharge shape. These results have helped to motivate planned changes to the DIII-D lower divertor to allow efficient pumping of a high triangularity double-null divertor shape.

2. Safety Factor Profile

The achievable value of β_N is observed to depend on the minimum value of q. Discharges for this study are produced by increasing the electron temperature (T_e) during the ramp up of the plasma current, thus reducing the rate of current penetration so that at the end of the current ramp, q_{min} remains relatively high, above 2.5 if the plasma is in H-mode during the ramp-up [2]. Either by adjusting the parameters during the discharge formation or by delaying the high beta phase, the target q profile can be varied and the achievable beta as a function of q_{min} observed.

The best illustration of the dependence of the beta limit on q_{min} comes from an experimental measurement of the no-wall beta limit, the stability limit for low toroidal mode number (n), ideal instabilities without the stabilizing effect of a conducting wall. The no-wall limit measurement is made by observing the effect on toroidal rotation and stability as the correcting current for nonaxisymmetric fields is removed. As a result of removing the correcting current, the drag of the nonaxisymmetric fields on toroidal plasma rotation increases. The rotation rate decreases below the level required for the conducting vacuum vessel wall to stabilize effectively, and, if the beta is above the no-wall limit, a low-n instability is observed. As a result of the presence of the conducting wall, the observed instability is not an ideal mode, but rather an $n = 1$ resistive wall mode (RWM) that grows on the time scale of magnetic field penetration through the vessel wall, a few milliseconds [4]. A series of discharges is run with different feedback regulated values of β_N and the highest β_N value at which no instability is observed is determined to be the no-wall limit.

The measured no-wall β_N limit decreases as q_{min} increases. The trend is the same for the $n = 1$ no-wall stability limit calculated for model equilibria as shown in Fig. 1. In this case, both the experimental and model equilibria are up/down symmetric double-null divertors with triangularity $\delta = 0.65$ and elongation $\kappa = 1.85$. Model equilibria were created with the TOQ [5] inverse-equilibrium code and stability was analyzed with the finite hybrid element code GATO [6]. Quantitatively, the modeled stability limits are somewhat higher than the measured values as a result of the differences between the experimental and model equilibria in parameters in the H-mode edge pedestal region and the sensitivity of the no-wall stability limit to these parameters. The H-mode pedestal [7] is the region in the several percent of poloidal flux closest to the plasma boundary where there is a rapid change in the plasma pressure. In this region there is a narrow peak in the pressure gradient which is expected to be accompanied by bootstrap current that produces a peak in the current density. The height and width of the pressure and current peaks and their distance from the plasma boundary modify the stability limit. For example, the no-wall β_N limit is found to change by 0.4 as a result of a 35% change in the peak pedestal current density. This difference in β_N values is comparable to the difference between the modeled and measured no-wall limits.

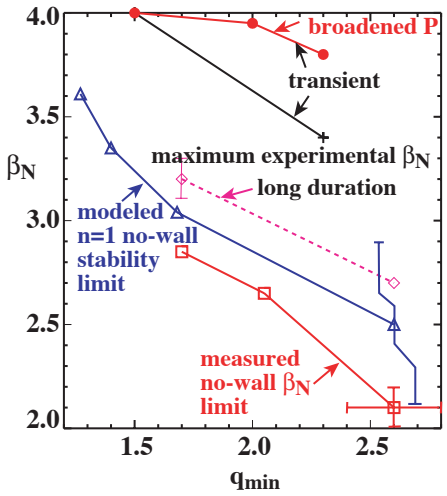

Fig. 1. The measured and modeled dependence of the β_N limit on the minimum safety factor.

The maximum achievable β_N values shown in Fig. 1 follow the same trend with q_{min} as the no-wall limit. However, this probably cannot be taken as an experimental indication of the scaling of the ideal-wall limit as the achieved β_N is often limited by an instability that is nonideal, such as a tearing mode. As shown in the figure, discharges with β_N 10% to 30% above the measured no-wall limit can be operated for the duration of the DIII-D discharge (up to several seconds) without occurrence of instabilities that significantly degrade confinement or beta. The high beta phase of discharges with β_N approaching the maximum achieved values is normally terminated by a tearing mode.

The choice to operate DIII-D steady-state scenario discharges with q_{95} near 5 rather than at lower values was based on the experimentally achievable β_N rather than the theoretical scaling of the stability limit. In experiments in which q_{95} was varied by changing the toroidal field at constant plasma current and discharge shape [2] the maximum achievable β_N was found to increase with q_{95}, changing from 3.4 to 4 by increasing B_t from 1.6 T (q_{95} = 4) to 1.85 T (q_{95} = 4.8). In contrast, the calculated scaling in model equilibria (Fig. 2) shows a decrease in both the no-wall and ideal-wall n = 1 limits with B_t (or q_{95}). The scaling depends somewhat on whether $q(0)$ is allowed to change as B_t is varied. (In these model equilibria $q(0) \approx q_{95}$.) In the model, if $q(0)$ is held constant, the decrease in the stability limit with B_t is weak. The scaling of the measured no-wall limit agrees with the modeling, as shown in the figure. When this measurement was made, the discharge setup was adjusted to keep $q(0)$ as constant as possible, but there was still a small change that, based on Fig. 2, is not large enough to account for the observed change in the no-wall limit. The increase in the maximum experimental β_N with B_t is apparently the result of the ability to operate closer to the ideal wall limit. The discharge at B_t = 1.6 T, β_N = 3.4 has β_N only slightly above the measured n = 1 no-wall limit, and for GATO prediction of stability, a conducting wall relatively far from the plasma at 2.5 times the minor radius is required. In contrast, the discharge at B_t = 1.85 T, β_N = 4 requires a conducting wall at approximately the location of the DIII-D vacuum vessel for a prediction of stability, indicating that this discharge was operated close to the ideal-wall beta limit.

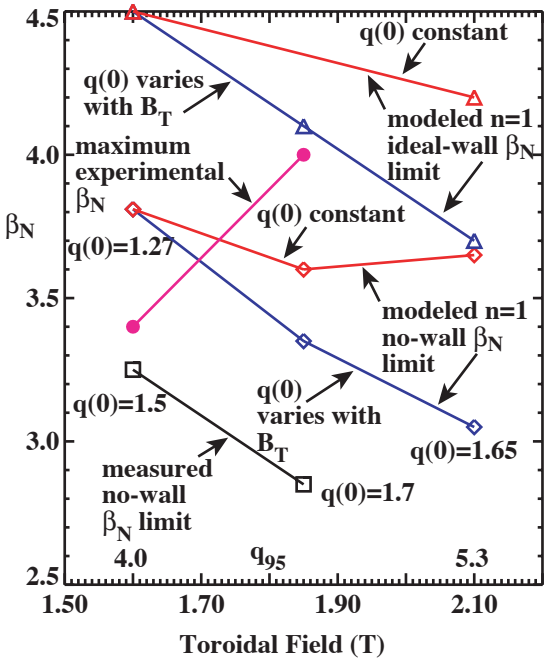

Fig. 2. Measured and modeled stability limits as a function of the toroidal field, or equivalently q_{95}, for fixed plasma current and discharge shape. Diamonds are the modeled no-wall limit and triangles are the modeled ideal-wall limit. Red lines denote cases in which $q(0) \approx q_{min}$ is held constant in the model, while blue lines are cases where $q(0)$ varied with toroidal field. Squares are the measured no-wall β_N limit and circles are the maximum experimentally achieved β_N.

3. Pressure Profile Width

Both modeling and experiment indicate that the low-n β_N limit can be increased by broadening the pressure profile, in the experiment nearly eliminating the dependence of the maximum achieved beta on q_{min}. The theoretical modeling [8] of the effect of the pressure profile width was focused on equilibria with high bootstrap current fractions, greater than 70%. The motivation was to explore the type of equilibrium that could eventually provide steady-state operation with a minimum of external current drive. Near the plasma boundary, the model pressure profiles have the hyperbolic tangent shape common in H-mode discharges [7] and pressure pedestal height scales as $P_{ped} \propto I_p^2\left(1+\beta_p\right)^{0.9}\left(1+\delta\right)^{2.11}\left(1+\kappa^2\right)^{-1.15}$, a form that roughly matches DIII-D data. In the core, the pressure gradient profile was modeled by a family of polynomials, $P'(\psi) = 1 + b\psi - (1+b)\psi^2$, with the coefficient b varied to obtain values of the pressure peaking factor, $P(0)/\langle P \rangle$ ranging from 2 to 4.5 (where $\langle P \rangle$ is the volume average pressure). An additional current that might be provided by an external noninductive current drive source was added to the bootstrap current to maintain q_{min} near, but above, 2 and $q(0) \approx 2.5$. Up/down symmetric double-null divertor equilibria were created with a range of discharge shape elongation, triangularity and squareness (see Section 4) and stability limits were calculated with an ideal wall at the location of the DIII-D vacuum vessel. Equilibria were created using the TEQ code [9,10] and stability was calculated using the DCON [11] and GATO codes.

A summary of the modeled scaling of the $n = 1$ β_N limit with the pressure peaking factor (Fig. 3) shows that there is a strong inverse dependence, $\beta_N^{limit} \propto [P(0)/\langle P\rangle]^{-1.3}$. The considerable variation in the data points on the figure results from the range of modeled discharge shapes. The modeling results suggest that for the broadest pressure profiles and the best discharge shape ($\kappa = 2.1$, $\delta = 0.8$) there should be stability to $n = 1$ with β_N near 6. However, for $P(0)/\langle P\rangle < 3$, $n = 2$ is predicted to set a lower stability boundary, with maximum $\beta_N \approx 5$ at $P(0)/\langle P\rangle \approx 2.2$. Figure 3 also shows the region in which recent experimental discharges have been produced. The maximum β_N values roughly follow the scaling predicted by the modeling.

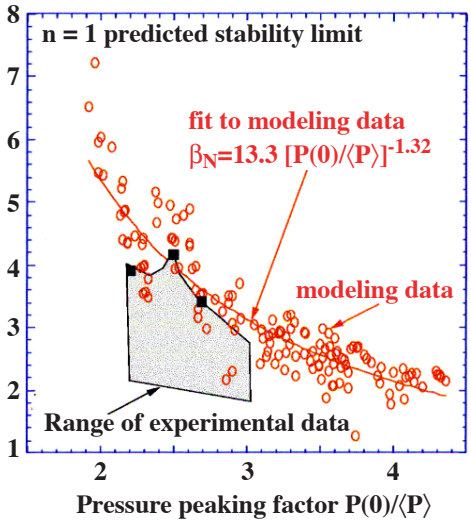

Fig.3. Calculated ideal n = 1 stability limit as a function of pressure peaking (circles). The scatter in the data points is a result of variation of the discharge shape. The squares are the measured values for discharges shown in Figs. 5 and 7.

In the experiment, a test of the stability dependence on the pressure profile was made by increasing the density profile width with an additional gas puff. The test was performed in discharges with $q_{min} > 2$ where the observed pressure peaking factor was normally relatively high. Figures 4 and 5 compare the pressure, density, temperature and toroidal rotation profiles and time evolution of two discharges, with and without the extra gas input to broaden the density profile. The profiles are compared at $t \approx 1.85$ s when both discharges have $q_{min} = 2.3$. Without the gas puff, $P(0)/\langle P\rangle = 2.7$ and $\beta_N = 3.5$ while with the extra gas, $P(0)/\langle P\rangle = 2.2$, $\beta_N = 3.8$ and $q_{min}\beta_N \approx 9$. Theoretical stability analysis indicates that the discharge with the broader pressure profile requires an ideal conducting wall at $1.65a$ for stability while the other discharge is predicted slightly more unstable, requiring the conducting wall at $1.5a$. Soon after 1.85 s, the discharge with the more peaked pressure disrupts while the other discharge continues and reaches $\beta_N = 4$ at $t \approx 2.15$ s when $q_{min} = 2$. Analysis indicates that the conducting wall must be inside $1.55a$ for stability. So, the broader pressure profile allows access to a higher β_N value for comparable q_{min} and allows higher achievable β_N with $q_{min} = 2$, comparable to what has been achieved at $q_{min} = 1.5$, although a somewhat lower pressure peaking factor is required ($P(0)/\langle P\rangle = 2.2$ versus 2.5). The DIII-D vessel is approximately equivalent to a conformal wall at $1.45a$, so during the highest beta phases both discharges are very close to the ideal-wall stability limit.

The time evolution of the toroidal rotation profile in the more peaked pressure profile discharge is consistent with the no-wall stability limit measurements described in Section 2. There is a factor of 2 decrease in rotation frequency that occurs between 1.3 and 1.4 s that cannot be accounted for by the 10% increase in density during the same period [for example, at $\rho \approx 0.7$ as shown in Fig. 5(b)]. The beginning of the rotation decrease correlates with the beginning of the portion of the discharge where β_N exceeds the no-wall stability limit, $\beta_N > 2.1$ (Fig. 1). This decrease in rotation is likely a result of increased drag above the no-wall beta limit by nonaxisymmetric magnetic field resulting from resonant amplification of the field by a marginally stable RWM [12]. The RWM is stabilized by the combination of toroidal rotation and active feedback stabilization using the DIII-D external n = 1 coil set.

In addition to the increase in the maximum beta, indications of changes in stability limits with the pressure profile width come from the time evolution of the toroidal rotation profile as β_N nears its maximum value and the manner of termination of the high beta phase. As the β_N nears its maximum value, beginning at about 1.7 s in both of the discharges shown in Fig. 5, the toroidal rotation in the outer half of the discharge decreases to a low level. For example, in the discharge with the more peaked pressure profile the rotation reaches a value near zero at $\rho = 0.7$ [Fig. 4(e)]. In the discharge with the broader pressure profile, though, this rotation frequency

decrease is the slowest and the minimum value isn't reached until $\beta_N \approx 4$, while in the other discharge the minimum rotation frequency occurs at $\beta_N \approx 3.5$. The rotation frequency decrease is likely the result of a growing amplitude of marginally stabilized resistive wall modes as beta increases. Evidence for this comes from the magnitude of the n = 1 component of the radial magnetic field measured outside the plasma with a set of saddle loops as shown in Fig. 6. Multiple spikes in the radial field represent brief periods of instability growth stabilized by the combination of the remaining rotation and the active feedback stabilization [4]. There is also a low level, continuous component of the radial field. The termination of the high performance phase of the two discharges differs. At about 1.85 s when $q_{min} \approx 2.3$ there is an $n = 1$ tearing-mode-type instability in both discharges. In the discharge with the more peaked pressure, this mode grows rapidly to a large amplitude and becomes locked, resulting in the disruption. In the discharge with a broader pressure profile, this mode exists only briefly, after which, β_N continues to increase until a continuous $n = 1$ mode appears, growing to large amplitude and significantly degrading confinement.

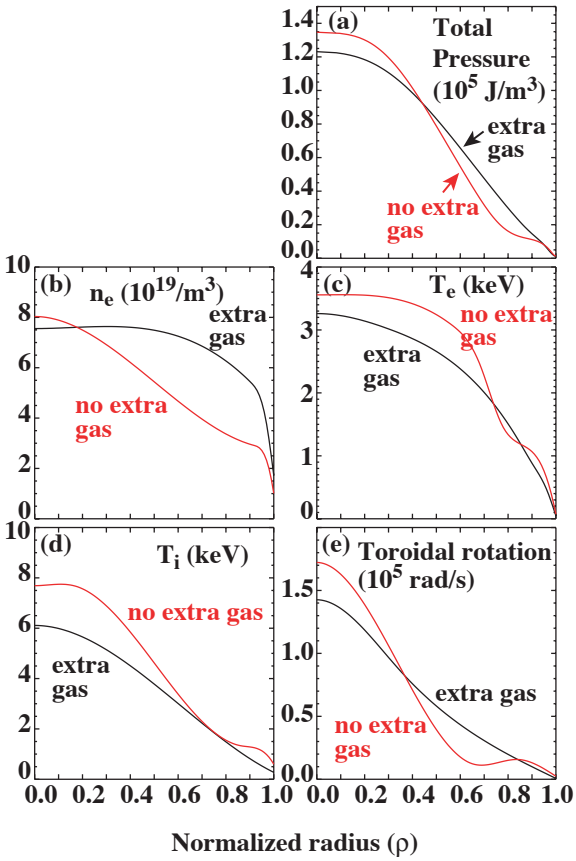

Fig. 4. Measured profiles at $\tau \approx 1.85$ s for discharges with and without an extra gas puff to broaden the density and pressure profiles. (a) Total plasma pressure, (b) electron density, (c) electron temperature, (d) ion temperature, (e) toroidal rotation frequency. (Shots 113699 and 114723.)

The modification of the toroidal rotation profile as the beta nears the ideal-wall limit results in a region of increased rotational shear that can modify the energy transport profile and the resulting density and temperature profiles, as illustrated in Fig. 4(e) for the more peaked pressure profile discharge. The ion and electron temperature profiles have regions of steeper gradient in the discharge core compared to the discharge with the additional gas puff which, at the time for which the profiles are shown in the figure, has not yet had a significant modification of the rotation profile. Later in the discharge, at higher beta, that discharge also showed evidence of steepening temperature profiles and steepening of the density profile as well. The result was an increase in $P(0)/\langle P \rangle$ of 5%–10% that probably had the effect of reducing the ideal-wall beta limit and the maximum achieved β_N.

4. Scaling with Discharge Shape

Both experimental and modeling studies of the low-*n* beta limits as a function of discharge shape have been conducted to assess the tradeoffs between divertor hardware geometry and achievable beta for operation of DIII-D steady-state scenario discharges. Presently, steady-state discharge studies are conducted with a double-null shape biased toward the divertor region at the top of the vessel where particle exhaust from higher triangularity shapes can be effectively pumped. The value of dRsep, the distance at the outer midplane between the separatrix flux surface of the upper X–point and the separatrix surface of the lower X–point is typically 1–2 cm.

In the experiment, it was demonstrated that increases in β_N can be obtained by operating with discharge shapes in which divertor exhaust pumping is presently not optimum but which could be compatible with a modest reconfiguration of the divertor hardware. Two discharge shapes were compared to the present pumping optimized shape which has $\kappa = 1.8$, $\delta_{upper} = 0.65$,

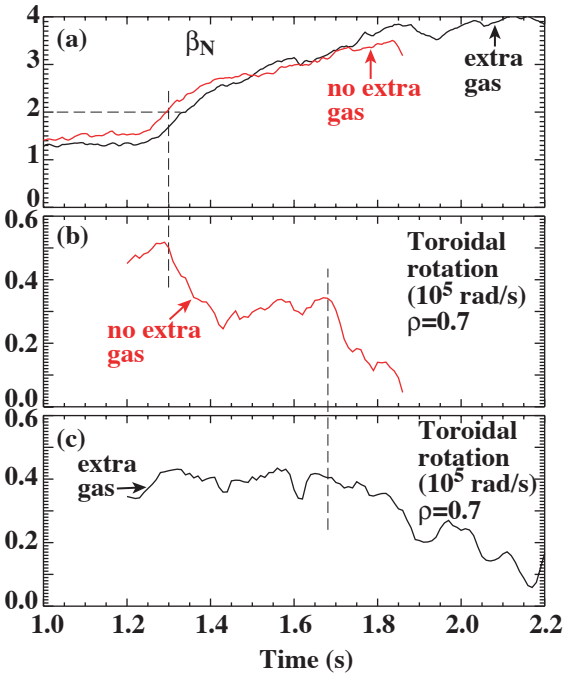

Fig. 5. Time evolution for discharges with and without an extra gas puff to broaden the density and pressure profiles. (a) Normalized beta, and toroidal rotation frequency at ρ ≈ 0.7 for the discharge (b) without and (c) with the extra gas puff. (Shots 113699 and 114723.)

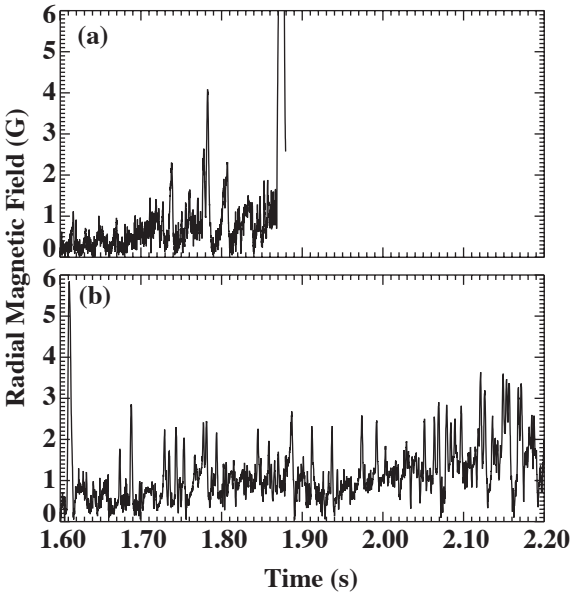

Fig. 6. Time evolution of the n = 1 component of the radial magnetic field for discharges (a) without and (b) with an extra gas puff to broaden the density and pressure profiles. (Shots 113699 and 114723.)

δ_{lower} = 0.32. Both were up/down symmetric double-null divertor configurations (dRsep = 0), one obtained by simply symmetrizing the standard pumping shape to κ = 1.92, δ_{upper} = 0.65, δ_{lower} = 0.77 and the other with slightly higher triangularity and elongation, κ = 2.0, δ_{upper} = 0.85, δ_{lower} = 0.78. The discharges were operated with the high beta phase when q_{min} ≈ 1.8. The maximum achieved beta values are plotted in Fig. 7 as a function of the shape parameter q_{95} I/(aB) [13]. The increase in β_N, from 3.65 to 4.1, came as a result of the change to the up/down symmetric double-null divertor. The two more strongly shaped discharges reached approximately the same β_N and in both cases the high beta phase was terminated by large edge-localized-modes (ELMs).

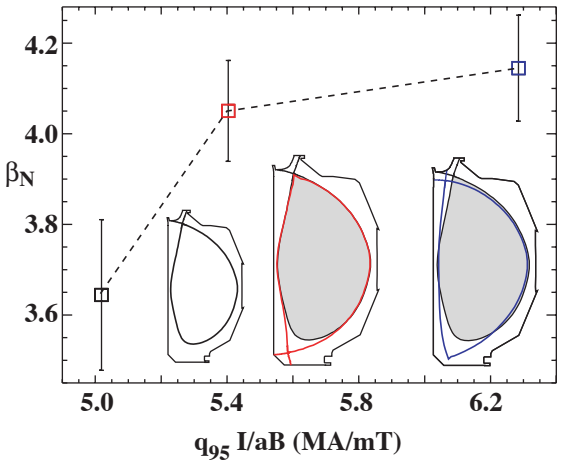

Fig. 7. Maximum achieved normalized beta in three discharges with different shape as a function of a parameter that increases with stronger shaping (e.g. higher κ and δ). The present pumping-optimized shape is at the left. The discharge shapes are shown within the DIII-D limiter outline as shaded insets. The two up/down symmetric shapes are also shown compared to the standard pumping-optimized shape.

This increase in the maximum achieved beta obtained by operating with dRsep = 0 is consistent with a separate measurement that was made of the dependence of the no-wall stability limit on dRsep. Discharge shapes with dRsep = 0 and dRsep = 3 cm were operated at q_{min} ≈ 1.7. The no-wall stability limit was observed to increase from β_N = 2.65 in the up/down asymmetric shape to 2.85 in the symmetric shape.

Modeling studies were conducted [8,14] to explore the changes in β_N stability limits that could be obtained through moderate changes to the typical discharge shape of κ = 1.8, δ = 0.65

and squareness [15] $\zeta = 0.05$ (see Fig. 8 caption) that could be accommodated in the DIII-D vacuum vessel. Examples of results are shown in Fig. 8. The $n = 1$ β_N limit increases with triangularity [Fig. 8(a)] as do the $n = 2$ and $n = 3$ limits. The stability limits generally increase with elongation as shown for $n = 1$ and 2 in Fig. 8(b), but the exact choice of squareness can modify this trend. In the example in the figure, for instance, at $\zeta = 0.2$ the stability limits decrease at $\kappa = 2.0$. The stability limits decrease with squareness [Fig. 8(c)], but there is an optimum value at $\zeta = 0.05$.

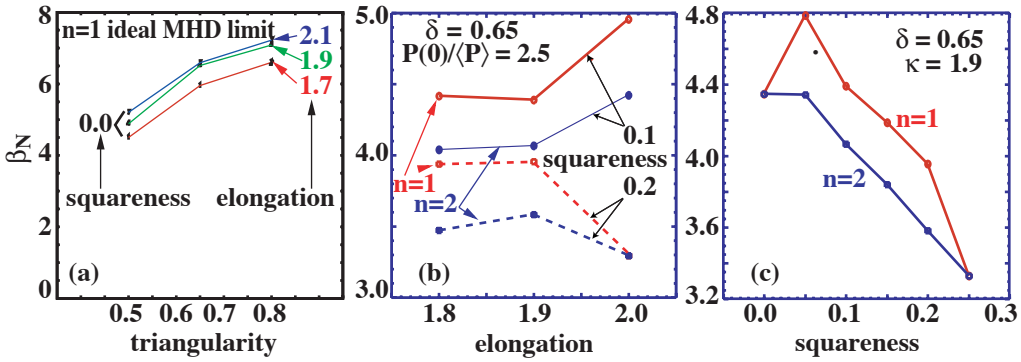

Fig. 8. Dependence of low-n β_N stability limits on discharge shape determined from model double-null divertor equilibria with dRsep = 0. In (a), $P(0)/\langle P\rangle = 2.3$ and $q_{min} \approx 1.5$. In (b) and (c), $P(0)/\langle P\rangle = 2.5$ and $q_{min} \approx 2$. In (a), generally higher β_N limits result from the lower pressure peaking and q_{min}. The discharge shape was modeled as having the form $R(\theta) = R_0 + a\cos(\theta + \sin^{-1}\delta \sin\theta)$, $Z(\theta) = \kappa a \sin(\theta + \zeta \sin 2\theta)$.

5. Conclusion

Using experiment and modeling, the effects of changes in the safety factor profile, the pressure profile, and discharge shape on the β_N limit for low-n instabilities in DIII-D advanced tokamak discharges have been explored. The goal of this work has been to find the best way to operate these discharges at high β_N and q in order to maximize the bootstrap current fraction for steady-state operation and the toroidal beta for fusion gain. In the experiment, the highest values of β_N are approximately 4 independent of q_{min} so that the maximum value of $q_{min}\beta_N \approx 9$ is obtained at the highest q_{min} value tested. The shape of the pressure profile is predicted by modeling to have a strong effect on the maximum β_N stable to low-n modes and experimental results from a test of this prediction are in agreement. DIII-D advanced tokamak discharges are routinely operated with β_N above the no-wall limit so that optimized correction of nonaxisymmetric fields is important to maintain toroidal rotation for resistive wall mode stabilization. At the highest values of β_N where the rotation is observed to decrease significantly, active feedback stabilization of the RWM is essential. This decrease in rotation at high β_N can result in pressure profile steepening, making it more difficult to produce broad pressure profiles at high beta. Modeling shows that increases in the elongation and triangularity in double-null discharge shapes can provide significant increases in the β_N limit. The results in the experiment, in which a double-null divertor shape is found to have a higher maximum β_N than the single-null divertor, pumping-optimized shape, are consistent with this modeling as the double-null shape has increased average triangularity and higher elongation.

Upcoming work in DIII-D is well positioned to follow the path to high β_N at increased values of q_{min} in steady-state advanced tokamak discharges pointed to by the results reported here [3]. Electron cyclotron and fast wave current drive will be used to control the current profile, in particular $q(0)$ and q_{min}. Planned conversion of part of the neutral beam power for injection counter to the plasma current direction will provide additional control of the rotation profile and ExB shear which, together with the current profile control, provides a possible mechanism for broadening the pressure profile through modification of energy transport. Modifications to convert the lower divertor pump to operate with higher triangularity will allow for operation with

strongly shaped double-null divertor discharges to take advantage of the increased beta limit. Use of the new nonaxisymmetric coils internal to the vacuum vessel [4] will provide improved correction of nonaxisymmetric fields and improved active RWM feedback control to allow steady-state operation close to the ideal-wall beta limit.

Acknowledgment

Work supported by U.S. Department of Energy under Contracts DE-FC02-04ER54698, W-7405-ENG-48, DE-0AC05-00OR22725, and DE-AC02-76CH03073 and Grants DE-FG03-01ER54615 and DE-FG02-89ER53297.

References

[1] BURRELL, K.H., Nucl. Fusion **43** (2003) 1555.
[2] WADE, M.R., *et al.*, Nucl. Fusion **43** (2003) 634.
[3] GREENFIELD, C.M., *et al.*, Phys. Plasmas **11** (2004) 2616.
[4] STRAIT, E.J., *et al.*, Phys. Plasmas **11** (2004) 2505.
[5] MILLER, R.L., *et al.*, Plasma Phys. Control. Fusion **40**, (1998) 753.
[6] BERNARD, L.C., *et al.*, Comput. Phys. Commun. **24**, (1981) 377.
[7] GROEBNER, R.J. and OSBORNE, T.H., Phys. Plasmas, **5** (1998) 1800.
[8] MAKOWSKI, M.A., *et al.*, "Effect of Profiles and Shape on Ideal Stability of Advanced Tokamak Equilibria," *Proc. of the 30th European Conference on Controlled Fusion and Plasma Physics*, St. Petersburg, 2003 (European Physical Society, Geneva, 2003), ECA Vol. 27A., P-2.113, and http://epsppd.epfl.ch/StPetersburg/PDF/P2_113.PDF.
[9] LODESTRO, L.L. and PEARLSTEIN, L.D., Phys. Plasmas **1** (1994) 90.
[10] PEARLSTEIN, L.D., *et al., Proc. 28th EPS Conf. on Controlled Fusion and Plasma Physics*, Funchal, 2001 (European Physical Society, Geneva, 2001), ECA Vol. **25A**, 1901.
[11] GLASSER, A.H. and CHANCE, M.S., Bull. Am Phys. Soc., **42** (1997) 1848.
[12] BOOZER, A.H., Phys. Rev. Lett. **86** (2001) 5059.
[13] LAZARUS, E.A., *et al.*, Phys. Fluids B **3** (1991) 2220.
[14] KESSEL, C.E., *et al.*, "Shape optimization for DIII-D advanced tokamak plasmas," *Proc. of the 30th European Conference on Controlled Fusion and Plasma Physics*, St. Petersburg, 2003 (European Physical Society, Geneva, 2003), ECA Vol. **27A**., P-4.044, and http://epsppd.epfl.ch/StPetersburg/PDF/P4_044.PDF.
[15] FERRON, J.R., *et al.*, Phys. Plasmas, **7** (2000) 1976.